Fourier Methods for Harmonic Scalar Waves in General Waveguides

Anders Andersson, Börje Nilsson, Thomas Biro

January 15, 2013

1 Introduction

Wave scattering in waveguides of different shapes is a classical problem in applied mathematics. The problem appears in many applications, in acoustics, optics, electro-dynamics and quantum physics.

When treating this problem mathematically, the task is to find solutions to the wave equation in some of its forms, and an essential part of this task is to solve Helmholtz equation

$$(\nabla^2 + k^2)p = 0 \tag{1}$$

in different geometries and with various boundary conditions.

For simple geometries, for example straight channels with hard or soft walls, the solutions are easily found in terms of Fourier series. Examples using this technique are found in any basic text on partial differential equations. For more complex geometries or boundary conditions, pure numerical methods or more precisely, finite element methods, have during recent years, due to evalution of both the methods and the computors, become the natural choice for solving Helmholtz equation.

However, motivated by both the mathematics and applications involving inverse wave scattering problems, we find it interesting to see what can be done with the classical semi-analytical Fourier methods, even when the geometries and the boundary conditions are complex.

The purpose of this article is exactly this, to investigate and to show how Fourier methods can be used to solve wave scattering problems in a waveguide with geometry and boundary conditions that exceed the ordinary school book examples. To be able to do that, we use a toolbox containing a set of methods:

- The Building Block Method makes it possible to divide a complicated geometry into several tractable parts.
- Different conformal mapping methods are used to further simplify the geometry.

- Reformulation of (1) assuming that the field can be expressed in Fourier series.
- Determination of numericially stable differential equations for reflection and transmission operators means that these can be determined for each part of the waveguide.
- Dirichlet-to-Neumann operators make it possible to formulate and solve numerically stable differential equations for the field in the waveguide.

Additional well-known tools such as mode matching, are necessary to solve general waveguide problems, but are not used in this article.

In an example taken from acoustics, i.e., the field in the waveguide is scalar, we show how these techniques kan be combined, in order to get the complete solution of Helmholtz equation in a general waveguide. The results in this example are then compared with the results when using commercial finite element software to solve the problem.

The plan of the paper is as follows: In Section 2, the mathematical basis for a Fourier solution is outlined and in Section 3, it is described how the field as well as reflection and transmission operators are determined in a single "block", using conformal mappings and different reformulations of equation (1). Section 4 shows how these blocks can be combined, using the Building Block Method. Section 5 contains the example problem and a detailed description of the techniques used to solve it. Finally, some final comments are included in Section 6.

2 Preliminaries

The problem under investigation is propagation of scalar harmonic waves in a waveguide V, in $\mathbb{R}^2$ or $\mathbb{R}^3$, of rather general shape. Acoustic notation is used where the sound pressure p solves Helmholtz equation

$$(\nabla^2 + k^2)p(\boldsymbol{r}) = 0, \ \boldsymbol{r} \in V, \tag{2}$$

in the interior V of the waveguide and fulfils a homogeneous boundary condition

$$\frac{\partial p}{\partial n} = \mathrm{i}k\beta p, \ \boldsymbol{r} \in \partial V, \tag{3}$$

on the boundary ∂V. Here, $k \in \mathbb{R}^+$ is the wavenumber, $\beta \in \mathbb{C}$, $\mathrm{Re}\,\beta \geq 0$ is the (normalized) surface admittance and $\widehat{\boldsymbol{n}}$ is the outward pointing normal to ∂V. Special cases of the boundary conditions are $\beta = 0$ (Neumann or hard) and $\beta = \mathrm{i}\infty$ (Dirichlet or soft). The formulation assumes the time dependence $\exp(-\mathrm{i}kc_0t)$ in the underlying wave equation. In addition to the

sound velocity c_0, the acoustic medium in the waveguide is characterized by the density ρ_0. Both c_0 and ρ_0 are constant.

The waveguide $V \subset \mathbb{R}^n, n = 2, 3$, consists of three parts: an inner bounded and connected part V_i and two straight semi-infinite parts V_L and V_R. An axial co-ordinate u is associated to the waveguide with the positive axis aligned with V_R and the negative with V_L. Fig. 1 depicts this waveguide schematically. Using the notation $\mathbb{R}^{\pm}_{u_0} = \{u \in \mathbb{R} : u \gtrless u_0\}$, the

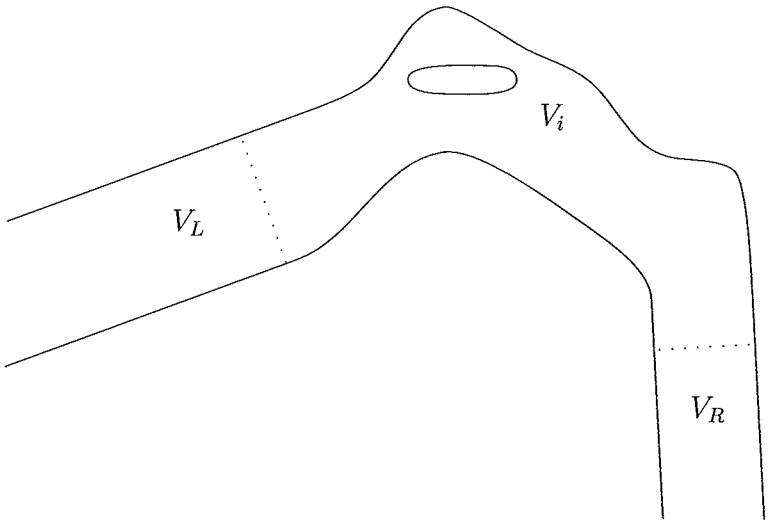

Figure 1: Waveguide $V = V_L \cup V_i \cup V_R$ consisting of straight parts V_L and V_R open to infinity and a bounded connecting part V_i.

straight waveguide parts are $V_\mathrm{L} = \Omega_\mathrm{L} \times \mathbb{R}^{-}_{u_\mathrm{L}}$ and $V_\mathrm{R} = \Omega_\mathrm{R} \times \mathbb{R}^{+}_{u_\mathrm{R}}$, where Ω_L and Ω_R are simply connected with boundary that is piecewise of class C^1. This means that Green's theorem is applicable. For simplicity it is assumed that the surface admittance $\beta = 0$ on $\partial V_\mathrm{L} \cap V$ and on $\partial V_\mathrm{R} \cap V$, whereas β can be non-vanishing and varying on V_i.

As a preparation for the definition of the scattering problem, we discuss propagation of waves in an infinite straight waveguide $V_\mathrm{s} = \Omega \times \mathbb{R}$, where Ω is Ω_L or Ω_R . If p solves (2) in V_s, p can be uniquely splitted into

$$p = p_- + p_+, \tag{4}$$

where

$$p_\pm = \sum_n p_n^\pm \mathrm{e}^{\pm \mathrm{i}\alpha_n u} \varphi_n(\boldsymbol{r}_\perp), \ \boldsymbol{r}_\perp \in \Omega. \tag{5}$$

Here, φ_n and $\lambda_n \geq 0$ are solutions to the eigenvalue problem

$$\begin{cases} (\nabla_\perp^2 + \lambda_n^2)\varphi_n(\boldsymbol{r}_\perp) = 0, \ \boldsymbol{r}_\perp \in \Omega \\ \dfrac{\partial \varphi_n}{\partial n}(\boldsymbol{r}_\perp) = 0, \ \boldsymbol{r}_\perp \in \partial\Omega \\ \int_\Omega \varphi_n^2(\mathbf{r}_\perp)\mathrm{d}\Omega = 1 \end{cases}, \tag{6}$$

$\nabla_\perp^2$ is the restriction of the Laplace operator to Ω, and

$$\alpha_n = \begin{cases} \sqrt{k^2 - \lambda_n^2}, \ k \geq \lambda_n \\ \mathrm{i}\sqrt{\lambda_n^2 - k^2}, \ k < \lambda_n \end{cases}. \tag{7}$$

We are interested in a solution p that has a finite (real and virtual) acoustic power in the axial direction and define to this end the function space

$$X_\pm = \left\{ p_\pm = \textstyle\sum_n p_n^\pm \mathrm{e}^{\pm \mathrm{i}\alpha_n u}\varphi_n(\boldsymbol{r}_\perp) : \sum_n |\alpha_n| \left|p_n^\pm\right|^2 < \infty \right\} \tag{8}$$

and $X = X_- \oplus X_+$. Then, $p_- \in X_-$, $p_+ \in X_+$ and $p \in X$.

If $p_+ \neq 0$, then we say that there is a source at $u = -\infty$, and if $p_- \neq 0$, there is a source at $u = +\infty$. Assume that there is a region $V_0 \subset V$, containing sources, i.e., where $(\nabla^2 + k^2)p \neq 0$, and that this source region is confined to the interval $u_- < u < u_+$. In physical terms, there should be only outgoing waves outside the source region, i.e., leftgoing to the left and rightgoing to the right. In order to couple this requirement to our definition of p_- and p_+, we formulate the following

Axiom 1.

For the solution to $(\nabla^2 + k^2)p = -q$ *in* V_s, *where* $q = 0$ *for* $u < u_-$ *and* $u > u_+$,

$$\begin{array}{l} p = p_-, \ \textit{when } u < u_- \textit{ and there is no source in } u = -\infty \\ p = p_+, \ \textit{when } u > u_+ \textit{ and there is no source in } u = +\infty \end{array}.$$

Comment 1 Axiom 1 makes it natural to denote p_- as leftgoing and p_+ as rightgoing.

Comment 2 Axiom 1 can be derived from physical principles: (a) According to the principle of vanishing absorption, k is replaced by $k + \mathrm{i}\varepsilon$, $\varepsilon > 0$, requiring that the solution p tends to zero when the distance to the source region tends to infinity; then the limit of vanishing ε is taken. (b) According to the principle of causality, which is a fundamental physical principle, asymptotic or stationary solutions for large t to the wave equation $(\nabla^2 - c_0^{-2}\partial^2/\partial t^2)p = -q(\boldsymbol{r})\mathrm{H}(t)\sin(kc_0 t)$ is studied, where $\mathrm{H}(t)$ is Heaviside's step function. For both cases a) and b), Axiom 1 follows with $p_\pm$ according to (5-7).

3 Solving the one-block problems

Wave scattering in a complicated geometry with varying boundary conditions can be treated as a series of simpler problem, using the so called Building Block Method, see Section 4. The method determines reflection and transmission oprerators for the waveguide, given that these operators have been determined for each section ("block") of the waveguide.

In this section, we show how reflection and transmission operators for a single block are established, but also, using a Dirichlet-to-Neumann formulation, how the acoustic wave field inside the block could be determined. When performing these calculations, interactions from the two ends of the block must be avoided, and hence, each block is assumed to be an infinitely long waveguide with parallel straight walls and constant boundary conditions outside some bounded transition region.

In each such geometry, the boundary value problem

$$\begin{cases} \left(\nabla^2 + k^2\right) p(x,y) = 0 & \text{in the waveguide,} \\ \dfrac{\partial p}{\partial n} = \mathrm{i}k\beta(t)p & \text{on the boundary,} \end{cases} \tag{9}$$

where β varies smoothly with some boundary parameter t, should be solved. For the sake of simplicity, we assume that one of the channel walls is hard, giving a Neumann boundary condition there.

We use a conformal mapping

$$F : w = u + \mathrm{i}v \to z = x + \mathrm{i}y$$

to transform the geometry into a straight horizontal channel $\{u \in \mathbb{R}, 0 \leq v \leq 1\}$ in the (u,v)-plane, see Fig. 2. After this transformation, Eq. (9) yields

$$\begin{cases} \left(\nabla^2 + k^2\mu(u,v)\right)\Phi(u,v) = 0 \\ \left.\dfrac{\partial\Phi(u,v)}{\partial v}\right|_{v=1} = \mathrm{i}kY(u)\Phi(u,1) \\ \left.\dfrac{\partial\Phi(u,v)}{\partial v}\right|_{v=0} = 0 \end{cases} \tag{10}$$

where $\mu(u,v) = |F'(w)|^2$ and $Y(u) = \beta(u)\,|F'(u+i)|$.

Following the techniques, outlined in [3], where an electro-magemtic scattering problem is treated, or [13], where similar problems from acoustics are solved, we expand $\Phi(u,v)$ in cosine Fourier series over v, assuming that

$$\Phi(u,v) = \sum_n \Phi_n(u)\varphi_n(u,v), \tag{11}$$

where $\varphi_n(u,v) = \cos(v\lambda_n(u))$ for functions $\lambda_n(u), \quad n \in \mathbb{N}$.

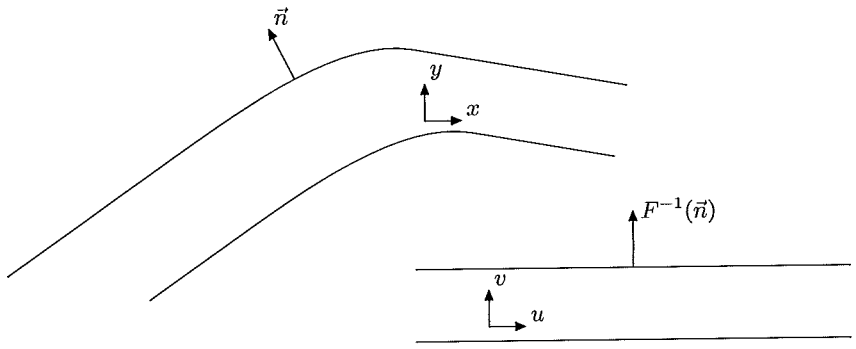

Figure 2: A single block in the $z = x + \mathrm{i}y$ plane and the $w = u + \mathrm{i}v$ plane.

The functions λ_n are determined by the boundary condition (10), from which follows that $\lambda_n(u)$, $n = 0, 1, \ldots$, are solutions to the equation

$$\lambda_n(u)\tan\big(\lambda_n(u)\big) = -\,\mathrm{i}kY(u). \tag{12}$$

By differentiating (12), it follows that

$$\lambda_n'(u) = \frac{-\,\mathrm{i}kY'(u)}{Q(u)} \tag{13}$$

and

$$\lambda_n''(u) = -\,\mathrm{i}k\left(\frac{Y''(u)Q(u) - Y'(u)Q'(u)}{\big(Q(u)\big)^2}\right) \tag{14}$$

where $(')$ stands for differentiating with respect to u and

$$Q(u) = \tan\big(\lambda(u)\big) + \lambda(u)\Big(1 + \tan^2\big(\lambda(u)\big)\Big).$$

From the expansions

$$v\sin(v\lambda_n(u)) = \sum_m \alpha_{mn}(u)\cos(v\lambda_m(u)), \tag{15}$$

$$v^2\cos(v\lambda_n(u)) = \sum_m \beta_{mn}(u)\cos(v\lambda_m(u)), \tag{16}$$

$$\mu(u,v)\cos(v\lambda_n(u)) = \sum_m \mu_{mn}(u)\cos(v\lambda_m(u)), \tag{17}$$

follows the infinite-dimensional ordinary differential equation

$$\boldsymbol{\Phi}''(u) - A(u)\boldsymbol{\Phi}'(u) - B^2(u)\boldsymbol{\Phi}(u) = 0, \tag{18}$$

where the infinite vector $\boldsymbol{\Phi} = (\Phi_1\Phi_2\Phi_3\ldots)^T$ and where the infinite matrices A and B^2 have elements

$$A_{mn}(u) = 2\alpha_{mn}(u)\lambda_n'(u) \tag{19}$$

and

$$B^2_{mn}(u) = \alpha_{mn}(u)\lambda_n''(u) + \beta_{mn}(u)\left(\lambda_n'(u)\right)^2 + \delta_{mn}\left(\lambda_n(u)\right)^2 - k^2\mu_{mn}(u). \tag{20}$$

3.1 Conformal mapping techniques

There are two indespensible requirements on the conformal mapping. When determining reflection and transmission operators for a single waveguide block, as well as the field inside the block, we must assume no interactions from the ends of the block. This is accomplished by treating the block as an infinite waveguide which is straight and has constant cross-sections outside some bounded region. We must therefore numerically construct a conformal mapping from a straight infinite channel to an infinite channel in which the walls at both ends are (at least) asymptotically straight and parallel. Furthermore, to avoid singularities in the operators A and B^2 in the differential equation (18), it follows from (10) that the mapping must have a bounded first derivative on the boundary, and additionally, from (13), (14), (19) and (20), bounded second and third derivatives if the boundary has non-zero amittance.

In [1] and [2], conformal mapping techniques, suitable for this situation, are developed. Both methods are built on the Schwarz–Christoffel mapping, which guarantees that the resulting channel walls are asymptotically straight and parallel towards infinity, and they both result in regions with smooth boundary curves, meaning that no singularities are introduced by the mapping. In [1], a suitable polygon, surrounding the region under consideration, is determined, and the conformal mapping is constructed by using the Schwarz–Christoffel mapping for that polygon. In [2], the factors in a Schwarz–Christoffel mapping are replaced by so called approximate curve factors that round the corners in a way that gives a smooth boundary curve.

3.2 Accomplishing stable equations

The differential equation (18) cannot be solved directly by numerical methods. However, there exist reformulations of (18) that are numerically stable for all but a countable set of k, i.e. for $k \notin \{k_1, k_2, k_3, \dots\}$. In this section, we describe two such reformulations, built on two different partitions of the wave field $\boldsymbol{\Phi}$.

Recall that the block is assumed to be an infintely long waveguide which is straight and has parallel hard boundaries outside some central transition region. Let Ω_L and Ω_R be the straight regions to the left and right respectively. In Ω_L and Ω_R, the operator A is zero, while B is constant. Assume that $B = B_-$ in Ω_L and $B = B_+$ in Ω_R. In Ω_L and Ω_R, B^2 is a real constant diagonal matrix, and to be consistent with standard theory for straight waveguides, the square roots of B^2 are chosen such that B_- and B_+ have either positive real or negative imaginary diagonal elements.

3.2.1 Determining Reflection and Transmission operators (The RT method)

Inspired by the partition $p = p_- + p_+$ in a straight waveguide where the two terms can be seen as representing waves marching from left to right and right to left respectively, we make the following definition: Let for all $u \in \mathbb{R}$, the wavefield

$$\boldsymbol{\Phi}(u) = (\Phi_1(u)\ \Phi_2(u)\ \ldots)^T = \boldsymbol{\Phi}^+(u) + \boldsymbol{\Phi}^-(u), \tag{21}$$

where $\boldsymbol{\Phi}^+(u)$ and $\boldsymbol{\Phi}^-(u)$ represent waves marching to the right and left respectively.

Let furthermore C and D be operators, depending on u, such that

$$\frac{\partial \boldsymbol{\Phi}}{\partial u}(u) = -C(u)\boldsymbol{\Phi}^+(u) + D(u)\boldsymbol{\Phi}^-(u), \tag{22}$$

for all $u \in \mathbb{R}$. C and D can be defined in many different ways, but they must be differentiable with respect to u, and since (18) must hold in Ω_L and Ω_R where $A(u) = 0$, it follows that $C = D = B_-$ in Ω_L and $C = D = B_+$ in Ω_R. We have used the definition

$$C(u) = D(u) = B_- + f(u)(B_+ - B_-), \tag{23}$$

where f is a smooth function that is 0 in Ω_L and 1 in Ω_R.

Define reflection and transmission operators R^+, R^-, T^+, T^-, such that for $u_1 < u_2$,

$$\begin{pmatrix} \boldsymbol{\Phi}^+(u_2) \\ \boldsymbol{\Phi}^-(u_1) \end{pmatrix} = \begin{pmatrix} T^+(u_2,u_1) & R^-(u_1,u_2) \\ R^+(u_2,u_1) & T^-(u_1,u_2) \end{pmatrix} \begin{pmatrix} \boldsymbol{\Phi}^+(u_1) \\ \boldsymbol{\Phi}^-(u_2) \end{pmatrix}. \tag{24}$$

This means that T^- and R^- transmits respectively reflects the left-going waves $\boldsymbol{\Phi}^-$, while T^+ and R^+ transmits respectively reflects the right-going waves $\boldsymbol{\Phi}^+$.

From (18), (21) and (22), it is possible to derive, for details see for example [13], the equation

$$\frac{\partial}{\partial u}\begin{pmatrix} \boldsymbol{\Phi}^+ \\ \boldsymbol{\Phi}^- \end{pmatrix} = \begin{pmatrix} J & K \\ L & M \end{pmatrix} \begin{pmatrix} \boldsymbol{\Phi}^+ \\ \boldsymbol{\Phi}^- \end{pmatrix}, \tag{25}$$

where

$$\begin{aligned} J &= (C+D)^{-1}\left(-C' - B^2 + (A-D)C\right), \\ K &= (C+D)^{-1}\left(D' - B^2 - (A-D)D\right), \\ L &= (C+D)^{-1}\left(C' + B^2 - (A+C)C\right), \\ M &= (C+D)^{-1}\left(-D' + B^2 + (A+C)D\right). \end{aligned} \tag{26}$$

For the determination of T^+ and R^+, we consider (24) assuming that there are no sources in Ω_R. Let $u_2 \in \Omega_R$ be constant and let $u = u_1$ vary. This means that $\boldsymbol{\Phi}^-(u_2) = 0$, and (24) simplifies to

$$\begin{cases} T^+(u_2,u)\boldsymbol{\Phi}^+(u) = \boldsymbol{\Phi}^+(u_2), \\ R^+(u_2,u)\boldsymbol{\Phi}^+(u) = \boldsymbol{\Phi}^-(u). \end{cases} \tag{27}$$

By differentiating (27) with respect to u, we get

$$\begin{cases} \dfrac{\partial T^+}{\partial u}(u_2,u)\boldsymbol{\Phi}^+(u) + T^+(u_2,u)\dfrac{\partial \boldsymbol{\Phi}^+}{\partial u}(u) = 0, \\ \dfrac{\partial R^+}{\partial u}(u_2,u)\boldsymbol{\Phi}^+(u) + R^+(u_2,u)\dfrac{\partial \boldsymbol{\Phi}^+}{\partial u}(u) = \dfrac{\partial \boldsymbol{\Phi}^-}{\partial u}(u), \end{cases} \tag{28}$$

and using (25) and (27) once more, the Ricatti equations

$$\begin{aligned} \frac{\partial R^+}{\partial u}(u_2,u) = -R^+(u_2,u)\big(J(u) + K(u)R^+(u_2,u)\big) \\ + L(u) + M(u)R^+(u_2,u) \end{aligned} \tag{29}$$

$$\frac{\partial T^+}{\partial u}(u_2,u) = -T^+(u_2,u)\big(J(u) + K(u)R^+(u_2,u)\big) \tag{30}$$

follow. For R^- and T^-, we proceed similarily assuming no sources in Ω_L, and deduce the equations

$$\begin{aligned} \frac{\partial R^-}{\partial u}(u,u_1) = -R^-(u,u_1)\big(M(u) + L(u)R^-(u,u_1)\big) \\ + K(u) + J(u)R^-(u,u_1), \end{aligned} \tag{31}$$

$$\frac{\partial T^-}{\partial u}(u,u_1) = -T^-(u,u_1)\big(M(u) + L(u)R^-(u,u_1)\big). \tag{32}$$

Using truncated matrices in place of J, K, L and M, these equations can be solved numerically with an ordinary differential equation solver. (29) and (30) are solved from right to left using $R^+(u_2,u_2) = 0$ and $T^+(u_2,u_2) = I$ as initial values, while (31) and (32) are solved from left to right, using $R^-(u_1,u_1) = 0$ and $T^-(u_1,u_1) = I$ as initial values. stability comments

3.2.2 Determining the field (The DtN method)

To determine the field inside a single block, we reformulate (18) using Dirichlet-to-Neumann operators, see also [11] and [4]. For this purpose, we make a different partition of $\boldsymbol{\Phi}$. Let

$$\boldsymbol{\Phi} = \boldsymbol{\Phi}_R + \boldsymbol{\Phi}_L, \tag{33}$$

where $\boldsymbol{\Phi}_R$ are waves with no sources to the right (in $+\infty$) and $\boldsymbol{\Phi}_L$ are waves with no sources to the left (in $-\infty$). Define Dirichlet to Neumann (DtN) operators Λ_R and Λ_L such that

$$\boldsymbol{\Phi}'_R(u) = -\Lambda_R(u)\boldsymbol{\Phi}_R(u), \tag{34}$$
$$\boldsymbol{\Phi}'_L(u) = \Lambda_L(u)\boldsymbol{\Phi}_L(u). \tag{35}$$

Φ_R and Φ_L are both satisfying (18), and by differentiating (34) and (35), the operator equations

$$\Lambda'_R(u) = \big(A(u) + \Lambda_R(u)\big)\Lambda_R(u) - B^2(u) \tag{36}$$
$$\Lambda'_L(u) = \big(A(u) - \Lambda_L(u)\big)\Lambda_L(u) + B^2(u) \tag{37}$$

follow. Since $A = 0$ in Ω_L and Ω_R,

$$\boldsymbol{\Phi}'_R(u) + B_-\boldsymbol{\Phi}_R(u) = 0, \quad \boldsymbol{\Phi}'_L(u) - B_-\boldsymbol{\Phi}_L(u) = 0, \qquad u \in \Omega_L, \tag{38}$$
$$\boldsymbol{\Phi}'_R(u) - B_+\boldsymbol{\Phi}_R(u) = 0, \quad \boldsymbol{\Phi}'_L(u) + B_-\boldsymbol{\Phi}_L(u) = 0, \qquad u \in \Omega_R, \tag{39}$$

which means that if truncated matrices are used in place of A and B^2, (36) and (37) can be solved numerically from right and left respectively, using the intial values $\Lambda_R(u_2) = B_+$ and $\Lambda_L(u_1) = B_-$, where $u_1 \in \Omega_L$ and $u_2 \in \Omega_R$. Finally, (34) and (35) are solved numerically from left and right respectively.

It is worth noticing that the Riccati equations (29-32) as well as (36-37) can for a countable set of k contain singularities for certain values of u and resist a numerical solution, for details and examples see for example [4]. However, these singularities appears for k values in the DtN equations (36-37) for which the RT equations (29-32) have no problem, so the different methods complete each other well. Furthermore, there exist numerical methods by which Riccati matrix equations are integrated across singularities, even when no knowledge about existance or placements of these is at hand, see for example [10].

4 Combining the Blocks - the Building Block Method

The Building Block Method (BBM), see [12], allows the determination of reflection and transmission operators for a combination of several sections ("blocks") of the waveguide, for which these operators are known.

Assume that two subsequent blocks Ω_1 and Ω_3, are connected by a region Ω_2 which is straight and with constant cross-section, see figure 3. For simplicity, we assume that Ω_2 is parallel to the x-axis. Furthermore, assume that reflection and transmission operators in matrix form for Ω_1 and Ω_2 are known. We use the following denotation:

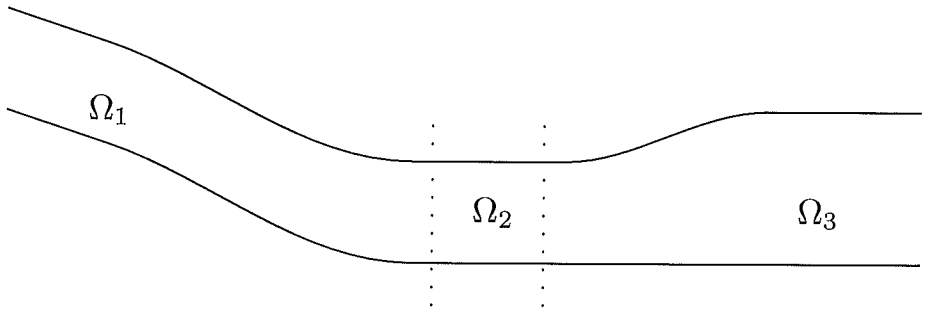

Figure 3: Waveguide divided in blocks. Ω_2 is straight and with constant cross-section.

Symbol	Explanation
R_1^+	Reflection operator for Ω_1 for waves entering from the left.
T_1^+	Transmission operator for Ω_1 for waves entering from the left.
R_1^-	Reflection operator for Ω_1 for waves entering from the right.
T_1^-	Transmission operator for Ω_1 for waves entering from the right.
R_3^+	Reflection operator for Ω_3 for waves entering from the left.
T_3^+	Transmission operator for Ω_3 for waves entering from the left.
R_{tot}^+	Reflection operator for $\cup_{j=1}^3 \Omega_j$ for waves entering from the left.
T_{tot}^+	Transmission operator for $\cup_{j=1}^3 \Omega_j$ for waves entering from the left.

You must define the choice of origin of basis for each matrix.

For the straight part Ω_2 having length ℓ and width a, we define the operator

$$S(x) = \begin{pmatrix} \mathrm{e}^{\mathrm{i}\alpha_0 x} & 0 & 0 & \cdots \\ 0 & \mathrm{e}^{\mathrm{i}\alpha_1 x} & 0 & \cdots \\ 0 & 0 & \mathrm{e}^{\mathrm{i}\alpha_2 x} & \\ \vdots & \vdots & & \ddots \end{pmatrix}, \quad 0 \le x \le \ell, \tag{40}$$

where $\alpha_n = \sqrt{k^2 - \dfrac{n^2\pi^2}{a^2}}$ and x is the horizontal distance from the border between Ω_1 and Ω_2.

Assume that a right-marching field $\boldsymbol{\Phi}^{\text{in}}$ is entering Ω_1 from the left, and that there are no sources to the right of Ω_3. Define operators $C^{\pm}$ such that at the border between Ω_1 and Ω_2 the right-marching and left-marching waves are $C^+\boldsymbol{\Phi}^{\text{in}}$ and $C^-\boldsymbol{\Phi}^{\text{in}}$ respectively. From standard theory for straight waveguides follows that in Ω_2 at position x, the field is

$$(S(x)C^+ + S^{-1}(x)C^-)\boldsymbol{\Phi}^{\text{in}}. \tag{41}$$

Consequently, at the border between Ω_2 and Ω_3, there are right-marching and left-marching waves $S(\ell)C^+\boldsymbol{\Phi}^{\text{in}}$ and $S^{-1}(\ell)C^-\boldsymbol{\Phi}^{\text{in}}$ respectively.

Since there are no sources to the right of Ω_3, $S^{-1}(\ell)C^- = R_3^+ S(\ell)C^+$, so $C^- = S(\ell)R_3^+ S(\ell)C^+$. But $C^+ = T_1^+ + R_1^- C^-$, and hence

$$\begin{aligned} C^+ &= \left(I - R_1^- S(\ell)R_3^+ S(\ell)\right)^{-1} T_1^+, \\ C^- &= S(\ell)R_3^+ S(\ell)C^+, \\ T_{\text{tot}}^+ &= T_3^+ S(\ell)C^+, \\ R_{\text{tot}}^+ &= R_1^+ + T_1^- C^-. \end{aligned} \tag{42}$$

The methods has been known since the end of the 1940:s [9] and is denoted the Building Block Method [12] in acoustic theory and cascade technique [8] in electromagnetic theory.

5 A numerical example

To illustrate the techniques, we solve the scattering problem and determine a low-frequency field in the waveguide shown in Fig. 4. The results, i.e., the

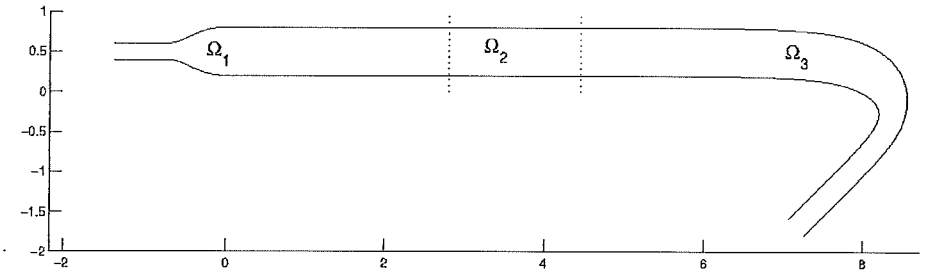

Figure 4: The waveguide in the example.

acoustic field in the waveguide given a known field entering from the left, as well as reflection as transmission operators for the waveguide, are calculated and compared with a finite element method solution.

5.1 Boundary conditions

In this geometry, we have run two test cases, (a) with hard walls, i.e., with zero admittance on all boundaries, and (b) with a varying admittance condition on the upper boundary. In the latter case, there is a smoothly and monotonuosly increasing admittance in the intervals $F_j([-2,-1]+\mathrm{i})$, a constant admittance $\beta = 0.5 + 0.5i$ in the intervals $F_j([-1,1]+\mathrm{i})$, and finally smoothly monotonously decreasing admittance in the intervals $F_j([1,2]+\mathrm{i})$, where the functions $F_j, j = 1,2$ are the conformal mappings defined in Section 5.2. The remaining boundaries are hard.

5.2 Conformal mappings

The region is divided into three disjunct parts. Ω_1 contains the change in cross-section to the left, the middle section Ω_2 is straight with constant cross-section, and Ω_3 contains the bending to the right.

For Ω_1, shown in Fig. 5(a), a conformal mapping is constructed using the approximate curve factor technique developed in [2]. The conformal mapping is $F_1 = f_1 \circ g_1$, where

$$f_1(w) = A \int_{w_0}^{w} \prod_{j=1}^{4} \left(\sqrt{(\omega + b_k \,\mathrm{i} - w_k)^2 - c_k^2} - b_k \,\mathrm{i} \right)^{\alpha_k - 1} \omega^{-1} d\omega + z_0, \quad (43)$$

and

$$g_1(w) = \exp(\pi w). \quad (44)$$

In (43), $A = 0.6/\pi$ to get the width 0.6 to the right, $\boldsymbol{\alpha} = (0.85, 1.15, 1.15, 0.85)^t$ to get inner angles of sizes 1.15π and 0.85π, $\boldsymbol{b} = \boldsymbol{c} = (1, 0.05, 0.05, 1)^t$ to get the corners appropriately rounded, and $\boldsymbol{w} = (-1, -a, a, 1)^t$, where $a = 0.008740$ has been numerically determined to get the width 0.2 to the left. Finally, w_0 is set to 2 and z_0 to $1 + 0.2i$ to position the waveguide in the complex plane.

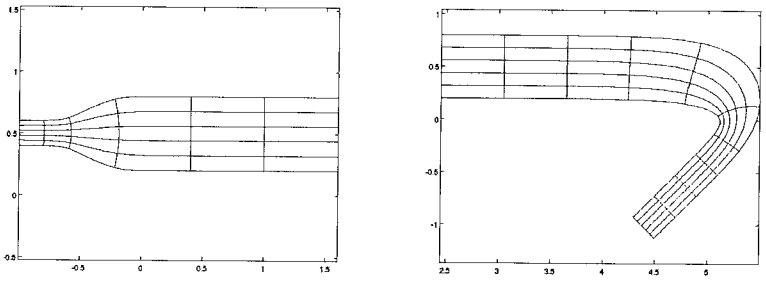

Figure 5: The two building blocks. The gridlines are images under the conformal mappings of $u = -5, -4, ..., 4, 5$ and $v = 0, 0.2, \ldots, 1$.

For Ω_3, shown in Fig. 5(b), the outer polygon method [1] is used to construct the conformal mapping. The mapping function is here $F_2 = f_2 \circ g_2$, where

$$f_2(w) = \int_{g_2(w_0)}^{w} \frac{(\omega - 1)^{\alpha - 1}}{(\omega + 1)^{\alpha - 1}(\omega - a)} d\omega + z_0 \quad (45)$$

and

$$g_2(w) = w^{(\varphi_2 - \varphi_1)/\pi} \, \mathrm{e}^{\mathrm{i}\varphi_1} + a, \quad (46)$$

with $A = 0.1501 \exp(3\pi \,\mathrm{i}/4)$, $\alpha = 7/4$, $\varphi_1 = 3\pi/10$, $\varphi_2 = 7\pi/10$, $a = -0.4632$, $w_0 = -7$ and $z_0 = 4.4485 + 0.2\,\mathrm{i}$.

5.3 Determination of the field, reflection and transmission operators

The acoustic fields inside Ω_1 and Ω_3 have been determined using the techniques described in Section 3.2.2. Simultaneously, reflection and transmission operators for Ω_1 and Ω_3 have been determined using the techniques in Section 3.2.1. All calculations have been made using 10×10 matrices in place of the operators in the differential equations (29)–(32) and (34–37) and a standard numerical ODE solver (`ode45`).

We have assumed a source at infinity to the left resulting in a right-marching wave $\mathbf{\Phi}_{\text{in}} = (1\ 0\ 0\ 0 \ldots)^t$ entering the waveguide from the left. No sources to the right is assumed.

The matrices $A(u)$ and $B^2(u)$ in (18), as well as the matrices J, K, L and M in (26) have been determined for $u = -5, -4.9, ..., 5$ in Ω_1, and for $u = -7, -6.9, ..., 7$ in Ω_3. Linear interpolation was then used in the ODE solvers to determine J, K, L and M in eqs. (29–32) and A and B^2 in eqs. (36) and (37) for u values not in this set.

Finally, the field in Ω_2 as well as reflection and transmission operators for the whole waveguide was calculated using the Building Block Method described in Section 4.

5.4 Results

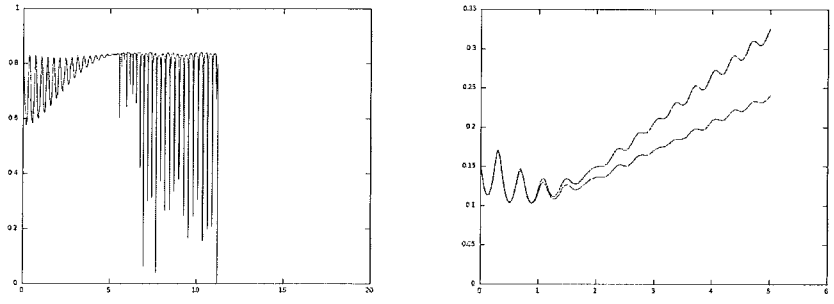

Figure 6: $|T(1,1)|$ for $\cup_{j=1}^{3}\Omega_j$ calculated for $k = 0..10$ with hard walls (left) and for $k = 0..5$ with admittance $0.5 + 0.5i$ (right).

We start this presentation with the results shown in Figure 6, where the absolute value of the first element in the transmission operator for the entire waveguide is calculated for a range of frequencies (k values), both with the Fourier methods presented in this article and with the finite element method. For hard boundaries, the results agree well for k values up to at least 15, but in the case with a non-zero admittance, the two methods disagree already for $k > 1$. The sources of this discrepancy will be discussed further in the

next section, but we will here present some results from the k intervals in which the methods agree mainly.

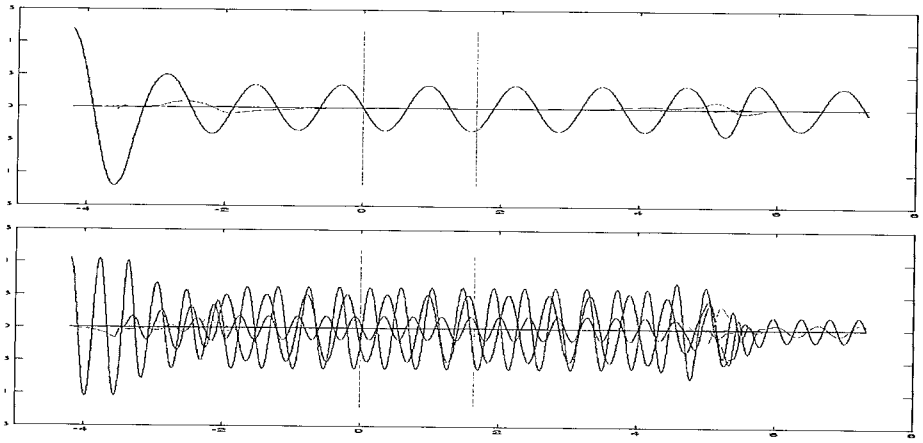

Figure 7: $\mathrm{Re}\,\Phi_1, \mathrm{Re}\,\Phi_2, \mathrm{Re}\,\Phi_3, \ldots$ for $k = 12$ and hard walls (above) and $k = 1$ and admittance as described in the article. Dotted vertical lines indicate borders between Ω_1, Ω_2 and Ω_3.

In Figure 7, $\mathrm{Re}\,\Phi_1, \mathrm{Re}\,\Phi_2, \ldots$ is plotted for $k = 5$, $k = 10$ and $k = 15$ in the hard wall case. The measure on the horizontal axis in the plot is the distance along the central curve in the waveguide. In Figure 8, a contour plot of $\mathrm{Re}\,p(x, y)$ is shown for $k = 15$ and hard walls, and in Figure 9, i similar plot is drawn for $k = 1$ and admittance conditions as described in Section 5.1.

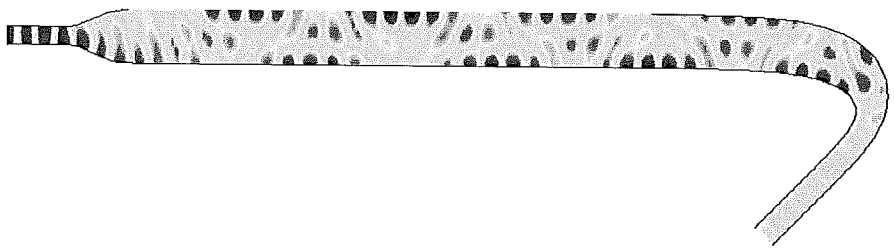

Figure 8: $\mathrm{Re}\,p(x, y)$ plotted for $k = 15$ and hard walls.

Note that in Ω_1, $\boldsymbol{\Phi}$ is calculated using the methods in Section 3.2.2, while in Ω_2, where it is calculated using (41) and (42), $\boldsymbol{\Phi}$ depends on the reflection and transmission operators found by the methods in Section 3.2.1. It is therefore interesting to compare $\boldsymbol{\Phi}$ in the right end of Ω_1 with $\boldsymbol{\Phi}$ in the left end of Ω_2, i.e. with $(A + B)\boldsymbol{\Phi}^{\mathrm{in}}$. This comparison is done in Table 1, and shows that the RT method and the DtN method confirm each other

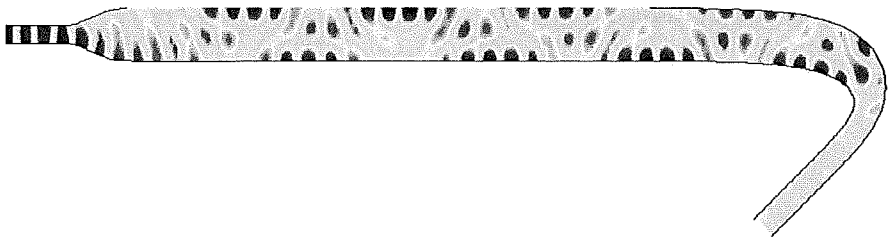

Figure 9: $\mathrm{Re}\, p(x, y)$ plotted for $k = 1$ and admittance conditions as described in Section 5.1.

well. The difference between the two results gives a hint of the accuracy of the calculations.

$k = 5$	$\boldsymbol{\Phi}_{\Omega_1}(\text{end})$	$\boldsymbol{\Phi}_{\Omega_2}(0)$	|difference|
Φ_1	$0.0113 + 0.4217\,\mathrm{i}$	$0.0115 + 0.4218\,\mathrm{i}$	$2 \cdot 10^{-4}$
Φ_2	$-0.0048 + 0.0077\,\mathrm{i}$	$-0.0048 + 0.0077\,\mathrm{i}$	$2 \cdot 10^{-5}$
$k = 10$	$\boldsymbol{\Phi}_{\Omega_1}(\text{end})$	$\boldsymbol{\Phi}_{\Omega_2}(0)$	|difference|
Φ_1	$-0.0654 - 0.3796\,\mathrm{i}$	$-0.0656 - 0.3794\,\mathrm{i}$	$3 \cdot 10^{-4}$
Φ_2	$0.4863 - 0.0468\,\mathrm{i}$	$0.4867 - 0.0472\,\mathrm{i}$	$6 \cdot 10^{-4}$
Φ_3	$0.0001 - 0.0003\,\mathrm{i}$	$0.0001 - 0.0003\,\mathrm{i}$	$2 \cdot 10^{-6}$
$k = 15$	$\boldsymbol{\Phi}_{\Omega_1}(\text{end})$	$\boldsymbol{\Phi}_{\Omega_2}(0)$	|difference|
Φ_1	$0.0761 + 0.1371\,\mathrm{i}$	$0.0763 + 0.1368\,\mathrm{i}$	$3 \cdot 10^{-4}$
Φ_2	$-0.2413 - 0.5671\,\mathrm{i}$	$-0.2417 - 0.5670\,\mathrm{i}$	$4 \cdot 10^{-4}$
Φ_3	$-0.2527 + 0.3930\,\mathrm{i}$	$-0.2525 + 0.3937\,\mathrm{i}$	$7 \cdot 10^{-4}$
$k = 20$	$\boldsymbol{\Phi}_{\Omega_1}(\text{end})$	$\boldsymbol{\Phi}_{\Omega_2}(0)$	|difference|
Φ_1	$0.0572 + 0.1007\,\mathrm{i}$	$0.0574 + 0.1008\,\mathrm{i}$	$2 \cdot 10^{-4}$
Φ_2	$0.1233 + 0.4054\,\mathrm{i}$	$0.1240 + 0.4049\,\mathrm{i}$	$8 \cdot 10^{-4}$
Φ_3	$0.1733 + 0.6416\,\mathrm{i}$	$0.1743 + 0.6419\,\mathrm{i}$	$1.1 \cdot 10^{-3}$
Φ_4	$-0.3960 + 0.2255\,\mathrm{i}$	$-0.3959 + 0.2266\,\mathrm{i}$	$1.1 \cdot 10^{-3}$

Table 1: Φ_1, Φ_2, Φ_3 and Φ_4 at the border between Ω_1 and Ω_2 calculated with two different methods for $k = 5, 10, 15, 20$.

A similar comparison is given in Table 2 where $\boldsymbol{\Phi}$ in the end of Ω_3 is compared to $T^{\text{tot}}\boldsymbol{\Phi}^{\text{in}}$ and with corresponding results from the FEM calculus.

6 Discussion and conclusion

The example problem in Section 5 is of course not a "general" waveguide. There are numerous possible boundary variations not commented so far. Below follows a list of some such problems and suggestions how to treat

$k = 5$	$\boldsymbol{\Phi}_{\Omega_3}(\text{end})$	$T^{\text{tot}}\boldsymbol{\Phi}^{\text{in}}$	|difference|
Φ_1	$-0.0744 + 0.3166\,\mathrm{i}$	$-0.0744 + 0.3166\,\mathrm{i}$	$4 \cdot 10^{-5}$
$k = 10$			
Φ_1	$0.0902 + 0.0420\,\mathrm{i}$	$0.0903 + 0.0421\,\mathrm{i}$	$1 \cdot 10^{-4}$
$k = 15$			
Φ_1	$0.0066 + 0.1879\,\mathrm{i}$	$0.0067 + 0.1879\,\mathrm{i}$	$1 \cdot 10^{-4}$
Φ_2	$0.0626 + 0.0580\,\mathrm{i}$	$0.0626 + 0.0580\,\mathrm{i}$	$1 \cdot 10^{-4}$
$k = 20$			
Φ_1	$0.1107 - 0.0280\,\mathrm{i}$	$0.1105 - 0.0281\,\mathrm{i}$	$2 \cdot 10^{-4}$
Φ_2	$-0.4216 - 0.0965\,\mathrm{i}$	$-0.4222 - 0.0957\,\mathrm{i}$	$1.0 \cdot 10^{-3}$

Table 2: Φ_1 and Φ_2 at the end of Ω_3 calculated with two different methods for $k = 5, 10, 15, 20$.

them:

The boundary has sharp vertices. When solving the one-block problems with the methods described in Section 3, we assume that the waveguide has smooth boundaries. Elsewise, the μ function in (10) will have singularities on the boundaries. However, as is illustrated in...

Sudden changes in the boundary conditions. A disadvantage with the Fourier methods seems to be that they require a boundary and boundary conditions with a high degree of smoothness. In the example in Section 5, this is the case. If not, the first and second derivatives of the λ functions, used in eqs. (19) and (20), will contain singularities. However...

Varying boundary conditions in both boundaries. In Section 3, we assumed that one of the boundaries was hard. This made it possible to develop the field in the waveguide in Fourier cosine series. If that is not the case...

Combinations of several different changes.

Three-dimensional waveguides. The methods are under certain conditions applicable even in three-dimensional problems. If the changes in geometry take place in at most two dimensions at the time,...

The most time-consuming part of the calculations is the determination of the matrices A and B^2 in (18) for a large set of u-values. For every value of u, $\lambda_n(u)$ for $n = 0, \ldots, N-1$ should be found by solving equation (12) numerically. The values of α and β in eqs. (15) and (16) can be determined

analytically, but for every u, N^2 numerical integrations are needed to determine the values of $\mu_{mn}(u)$ in eq. (17). For values of u, corresponding to hard boundaries, $\lambda_n = n\pi$ and the μ coefficients can be calculated using Fast Fourier Transforms, but for values of u corresponding to boundaries with admittance, a comparatively slow numerical integration must be used for each matrix element.

However, as is seen in Figure..., in the k intervals where the Fourier method and the finite element method agree, the size of the truncated matrices seems not to be the critical. In the figure, $\left|T^{\text{tot}}(1,1)\right|$ is plotted over increasing matrix sizes from 2×2 to 30×30. The results seem to be stable to three significant figures already for 5×5 matrices.

As a reference and comparision, the problem in the example has been solved using commercial software for the finite element method (FEM). It turns out, see Figure 6, that with hard boundaries, the correspondence is good for a relatively large frequency domain, but that for non-hard boundaries, the two methods correspond only for low frequencies.

It is beyond the scope of this paper to fully investigate the sources of the disparities revealed in Figure 6. It is a well-known fact that the number of mesh elements required to get an accurate FEM solution to a wave scattering problem increases rapidly with growing fequencies, see for example [7] or [6]. However, the FEM results seem to be stable under a change of mesh size in the frequency interval we are investigating.

On the other hand, the required matrix size in the Fourier methods developed in this article depends also on the frequency, Even if the simple stability test mentioned above indicates a stable solution already for comparably small matrices, it is worth noticing that for non-hard boundaries, the ommited matrix elements could be of substantial size. A thorough examination of the A and B^2 matrices in (18) and their origins exposes some interesting details. The cosine series of a sine function converges slowly, which means that the values of α_n are relatively large even for large values of n. For u-values corresponding to varying boundary conditions, the values of λ' and λ'' are substantial, giving that the elements of A and B^2 could be of a considerable size, even far from the matrix diagonal. This means that when truncating these matrices to a tractable size, important information might get lost.

There are ways to overcome problems related to the Gibbs phenomenon in Fourier series, see for example [5]. However, we have not in the example shown here implemented any such methods.

Even though an extensive error-checking has been applied to the code, we cannot completely disregard the possibility of an erroneous computer implementation of the mathematical methods as an explantion to the discrepancy between the results of the two methods.

At the present stage, we can just conclude that the semi-analytical Fourier methods discussed in this article are well working alternatives for

wave scattering problems in the low-frequency domain. More precise bounds for this domain are still to be determined.

References

[1] Anders Andersson. Schwarz–Christoffel mappings for nonpolygonal regions. *SIAM J. Sci. Comput.*, 31(1):94–111, 2008.

[2] Anders Andersson. Modified Schwarz-Christoffel mappings using approximate curve factors. *J. Comp. Appl. Math.*, 233(4):1117 – 1127, 2009.

[3] Anders Andersson and Börje Nilsson. Electro-magnetic scattering in variously shaped waveguides with an impedance condition. In *AIP Conference Proceedings: 3rd Conference on Mathematical Modeling of Wave Phenomena*, volume 1106, pages 36–45. AIP, 2009.

[4] L. Fishman, A. K. Gautesen, and Z. Sun. An exact, well-posed, one-way reformulation of the Helmholtz equation with application to direct and inverse wave propagation modeling. In *New Perspectives on Problems in Classical and Quantum Physics: A Festschrift in Honor of Herbert Überall*, pages 75–97. CRC Press, 1998.

[5] David Gottlieb and Chi-Wang Shu. On the Gibbs phenomenon and its resolution. *SIAM Rev.*, 39(4):644–668, 1997.

[6] Isaac Harari. A survey of finite element methods for time-harmonic acoustics. *Computer Methods in Applied Mechanics and Engineering*, 195(1316):1594 – 1607, 2006.

[7] Frank Ihlenburg. *Finite element analysis of acoustic scattering*, volume 132 of *Applied Mathematical Sciences*. Springer-Verlag, New York, 1998.

[8] D. S. Jones. *Acoustic and electromagnetic waves*. Oxford University press, Oxford, 1986.

[9] D. M. Kerns. Basis of the application of network equations to waveguide problems. *J. Res. natn. Bur. Stand.*, 42:515–540, 1949.

[10] Ren-Cang Li and William Kahan. A family of anadromic numerical methods for matrix Riccati differential equations. *Math. Comp.*, 81(277):233–265, 2012.

[11] Ya Yan Lu. Exact one-way methods for acoustic waveguides. *Math. Comput. Simulation*, 50(5-6):377–391, 1999.

[12] B. Nilsson and O. Brander. The propagation of sound in cylindrical ducts with mean flow and bulk reacting lining - IV. Several interacting discontinuities. *IMA J. Appl. Math*, 27:263–289, 1981.

[13] Börje Nilsson. Acoustic transmission in curved ducts with various cross-sections. *Proc. R. Soc. Lond. A*, 458:1555–1574, 2002.